Yttria-stabilized zirconia/SrTiO3 oxide heteroepitaxial interface with symmetry discontinuity

M. Scigaj, N. Dix, M. Cabero, A. Rivera-Calzada, J. Santamaria, J. Fontcuberta, G. Herranz, and F. Sánchez

Citation: Applied Physics Letters **104**, 251602 (2014); doi: 10.1063/1.4885089
View online: http://dx.doi.org/10.1063/1.4885089
View Table of Contents: http://scitation.aip.org/content/aip/journal/apl/104/25?ver=pdfcov
Published by the AIP Publishing

Yttria-stabilized zirconia/$SrTiO_3$ oxide heteroepitaxial interface with symmetry discontinuity

M. Scigaj,[1,2] N. Dix,[1] M. Cabero,[3] A. Rivera-Calzada,[3] J. Santamaria,[3] J. Fontcuberta,[1] G. Herranz,[1] and F. Sánchez[1,a)]

[1]*Institut de Ciència de Materials de Barcelona (ICMAB-CSIC), Campus UAB, 08193 Bellaterra, Barcelona, Spain*
[2]*Dep. de Física, Universitat Autònoma de Barcelona, Campus UAB, 08193 Bellaterra, Barcelona, Spain*
[3]*GFMC, Depto. de Física Aplicada III, Facultad de Física, Universidad Complutense, 28040 Madrid, Spain*

(Received 3 April 2014; accepted 13 June 2014; published online 24 June 2014)

We show that yttria-stabilized zirconia (YSZ) films deposited on structurally dissimilar $SrTiO_3$(110) substrates exhibit two-dimensional layer-by-layer growth. We observed that, up to a thickness of about 15 nm, the square (001) basal plane of the cubic YSZ grows epitaxially on the rectangular (110) crystallographic plane of $SrTiO_3$ substrates, with [110]YSZ(001)// [001]$SrTiO_3$(110) epitaxial relationship. Thus, the heterointerface presents symmetry discontinuity between the YSZ(001) film and the lower surface symmetry $SrTiO_3$(110) substrate. Beyond this specific case, we envisage similar approaches to develop other innovative oxide interfaces showing similar crystal symmetry discontinuities. © *2014 AIP Publishing LLC*.
[http://dx.doi.org/10.1063/1.4885089]

In heteroepitaxial growth of oxidefilms on crystalline substrates, the structural and electronic mismatch between the two crystalline materials causes profound effects on the film and on the interface. The structural mismatch induces elastic deformation of the film, and the selection of a particular substrate permit obtaining a desired lattice strain, with impact on the functional properties of the oxide thin film.[1] On the other hand, the interface itself can be the source of functional properties, different from those of substrate and film.[2] The most significant example is probably the electron liquid at the interface between the $LaAlO_3$ and $SrTiO_3$ (STO) insulators, usually explained by electron accumulation at Ti 3d bands, driven by the polar discontinuity.[3]

Most of the research on emergent properties from oxide interfaces is focused on (001)-oriented structures, but as recently pointed by Chakhalian *et al.*,[4] innovative interfaces would offer opportunities to explore new effects not seen along (001). This can be realized, for example, by achieving controlled growth of (110)- and (111)-oriented perovskites, as demonstrated with (110) and (111) $LaAlO_3$ films[5] or with (111) $LaFeO_3$-$LaCrO_3$ superlattices.[6] In these interfaces (A and B correspond to cations of ABO_3 perovskites), the film (F) maintains the orientation of the substrate (S), i.e., F(001)/S(001), F(110)/S(110), or F(111)/S(111) and thus the atomic stacking sequence (…A_FO-B_FO_2/A_SO-B_SO_2… for the (001), as example) across the interface. However, interface phenomena between oxides having cubic crystal structure (or permitting pseudocubic indexation) with different out-of-plane orientation of film and substrate, F(h′k′l′)/S(hkl) with different Miller indexes of their respective cubic cells, (h′k′l′) ≠ (hkl), remain unexplored.

Because of the symmetry rupture inherent to the F(h′k′l′)/S(hkl) orientational relationship, such interfaces could be the source of emerging properties. However, the degradation of the crystalline quality of heteroepitaxial oxide films with cubic crystal structure is common when its out-of-plane orientation changes respect to the substrate. For example, (110) films grown on (001) substrates exhibit crystal variants because the two-fold symmetry of the (110) surface of the film is lower than the four-fold of the (001) surface of the substrate,[7] which is confirmed experimentally with $SrRuO_3$(110)[8] and $SrTiO_3$(110)[9] on yttria-stabilized zirconia (YSZ(001)), or Sr(Ti,Fe)O_3 (110) on CeO_2(001).[10] Therefore, the usual (001) oriented substrates are not convenient for obtaining single-crystalline F(h′k′l′)/S(hkl) interfaces with (h′k′l′) ≠ (hkl). However, the reverse situation, in which a (001) film is grown on a (110) substrate, could permit having films free of crystalline variants thus allowing to obtain single domain interfaces. Here, we will show that single domain YSZ(001) films can be grown layer-by-layer on (110)-oriented $SrTiO_3$ substrates, presenting discontinuity of the crystal symmetry in the interface plane and discontinuity of the atomic stacking across it.

The STO(110) substrates were treated in a dedicated furnace at 1100 °C for 2 h in air to obtain a morphology of terraces and steps.[11] The YSZ films were grown by pulsed laser deposition ($\lambda = 248$ nm, 1 Hz repetition rate) assisted with reflection high energy electron diffraction (RHEED) operating at 30 kV. The substrates were heated up to the deposition temperature (850 °C) under an oxygen partial pressure P_{O2} of 0.1 mbar, being the YSZ films deposited at $P_{O2} = 10^{-4}$ mbar. The RHEED intensity oscillations of the specular spot were recorded with the incidence angle of the electron beam around 0.9°, being the STO[001] the azimuthal direction. Films 16, 32, and 64 monolayers (ML) thick were prepared using the appropriate number of laser pulses. The cooling procedure involved $P_{O2} = 0.3$ mbar from 850 °C to 750 °C and 200 mbar from 750 °C to room temperature with a dwell time of 1 h at 600 °C. Epitaxial relationships were determined by X-ray diffraction (XRD) using CuK_α radiation. Atomic force microscopy (AFM) in dynamic mode was used to characterize the surface morphology (images were

a)fsanchez@icmab.es

analyzed using the Gwyddion software[12]). The sketches of the atomic arrangement were prepared with the VESTA software.[13]

The RHEED patterns of the substrates (Figure 1(a)) exhibit specular spot, Bragg spots on the 0th Laue circle, and Kikuchi lines, signaling high crystalline order at the surface. The intensity of the specular spot was monitored during YSZ growth (Figure 1(e)). After the drop of the intensity when deposition starts, oscillations are observed. The first 4–5 oscillations are ill defined, particularly in the t = 32 ML film, but subsequent oscillations present high amplitude. The reduction of amplitude in the first oscillations, usually observed in RHEED monitoring of heteroepitaxial growth,[5,14] is likely due to interference between electrons reflected at the film surface and at the film-substrate interface. When increasing further the thickness the oscillations become clear, indicating that YSZ grows by layer-by-layer two-dimensional mechanism on the STO(110) substrate. Although there is a progressive damping of the oscillations, they were intense enough to permit stopping the deposition exactly at the maximum of an oscillation for the two thinnest films, after growth of 16 and 32 ML. In the case of the thickest film, deposition was stopped after nominal growth of 64 ML. At the end of the depositions, the RHEED patterns only present streaky YSZ Bragg spots (the corresponding to the t = 64 ML film, recorded along the YSZ[110]/STO[001] direction, is shown in Figure 1(b)) signaling that the surface is flat. The patterns along YSZ[−110] (Figure 1(c)) and YSZ[010] (Figure 1(d)) evidence the in-plane four-fold symmetry of the YSZ(110) film surface, in contrast with the two-fold symmetry of the STO(110) substrate surface.

The XRD $\theta/2\theta$ scan around symmetrical reflections of the 32 ML-thick sample (Figure 2(a)) shows high intensity peaks corresponding to the (ll0) reflections of the STO substrate as well as lower intensity YSZ(002) and YSZ(004) reflections. The out-of-plane YSZ lattice parameter determined from the position of the (004) reflection is 5.169(2) Å, slightly larger than the bulk value of around 5.14 Å.[15,16] The (00l) orientation of the YSZ film is compatible with the four-fold in-plane symmetry observed by RHEED. In the case of the thickest film (64 ML), a second peak at $2\theta^\circ \sim 30^\circ$ indicates the existence of crystallites with (111) orientation; from the intensity of XRD peaks its amount is estimated to

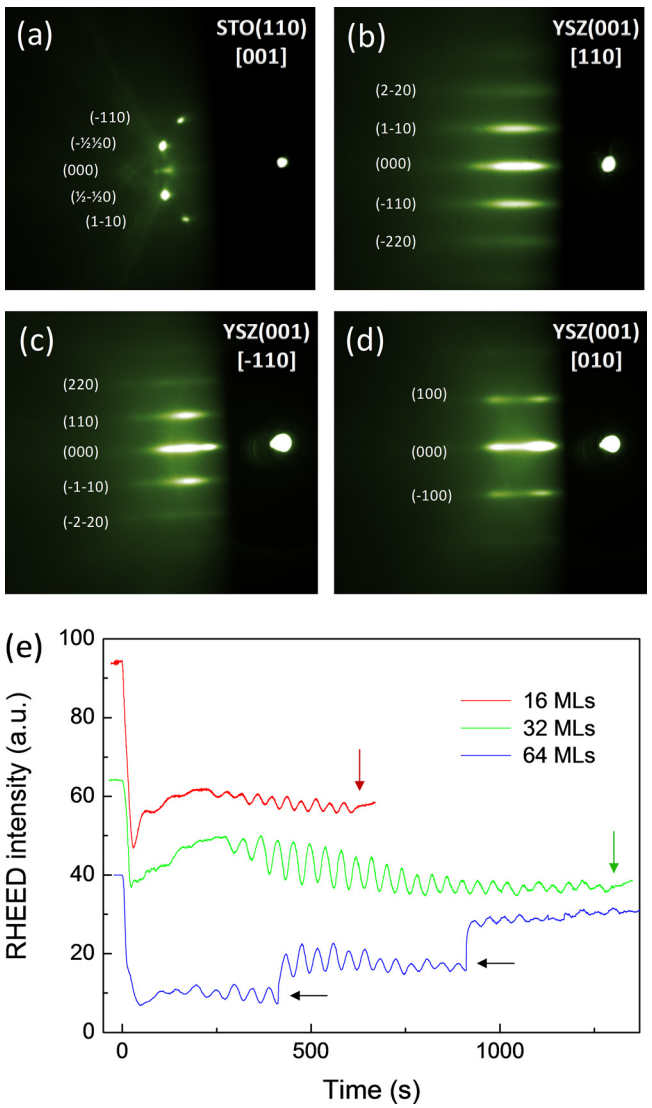

FIG. 1. (a) RHEED pattern of the STO(110) substrate, taken along STO[001] at room temperature and base pressure. (b) RHEED pattern at the end of the growth of the 64 MLs-thick YSZ film, taken along YSZ[110] at 850 °C under $P_{O2} = 10^{-4}$ mbar. (c) and (d) were taken along [−110]YSZ, and [010], respectively, at room temperature and base pressure, after air exposure of the sample. The barely appreciated arc is an instrumental artifact, caused by the small pinhole of the tube used in the high-pressure RHEED setup. (c) and (d) were recorded with changes in the optical setup of the CCD camera respect the conditions used for (a) and (b). (e) Intensity of the RHEED specular spot during deposition of YSZ films: 16 ML, 32 ML, and 64 ML; in the last case only data corresponding to the beginning of the growth is shown, with the horizontal arrows indicating that the intensity of the primary electrons beam was increased manually. Vertical arrows indicate the end of the deposition of the 16 and 32 ML films.

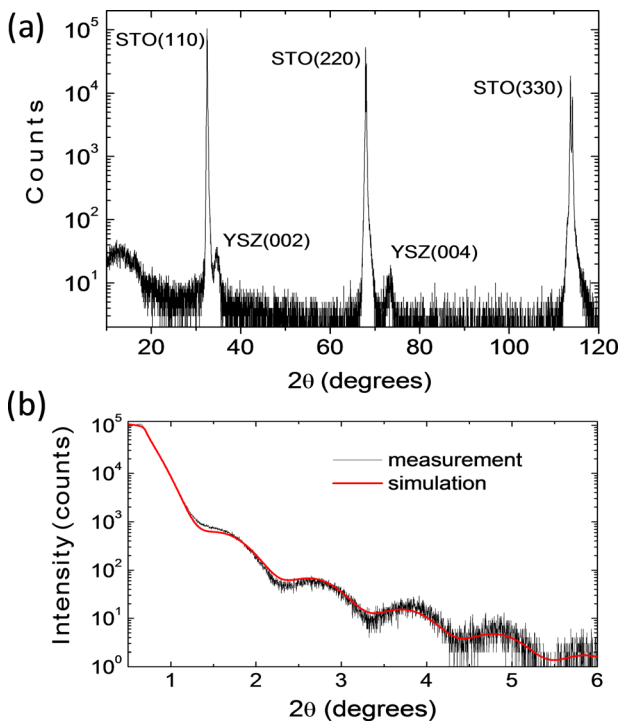

FIG. 2. (a) θ-2θ XRD scan of the 32 ML-thick YSZ film. (b) X-ray reflectivity data corresponding to the same sample; the simulation (red curve) is computed for a YSZ thickness of 82.1 Å. In (a), the broad feature at low angles (2θ below 20°) comes from the sample plastic holder used from the measurement.

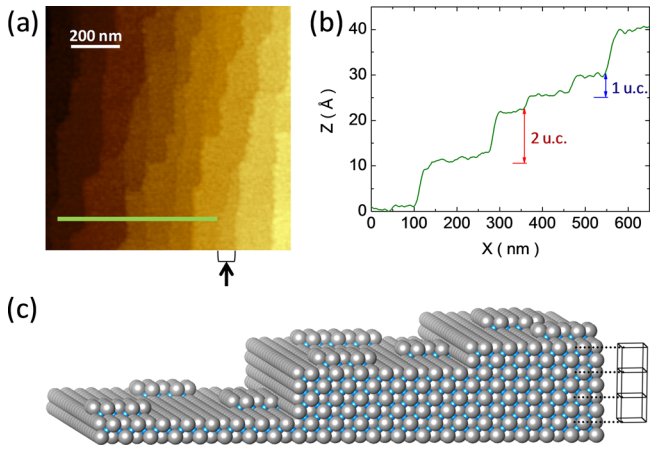

FIG. 3. (a) AFM topographic image of the 32 ML-thick YSZ film. The corresponding height profile along the line is depicted in the panel (b). (c) Sketch of the morphology at the beginning of the growth of a new monolayer being a half of a unit cell.

be below around 10%, small enough not to cause any observable additional spots in the RHEED patterns. The thickness of the film was determined by X-ray reflectometry. In Figure 2(b), we show the measurement of the 32 ML film, being the corresponding thickness 82.1 Å, thus very close to the thickness of 16 unit cells of YSZ (16×5.169 Å $= 82.7$ Å). Interestingly, the relation between the number of the RHEED oscillations (monolayers) and thickness, confirmed with other samples, implies that in the layer-by-layer mechanism each monolayer corresponds to half of a unit cell of YSZ.

The AFM topographic image of the 32 ML-thick sample is depicted in Figure 3(a). The roughness is very low (rms = 2 Å) and terraces and steps are appreciated. Terraces are covered by a dense distribution of two-dimensional islands of very small lateral size around 20 nm. The line profile in Figure 3(b) shows steps one unit cell high as well as others with a height of two unit cells. Moreover, the contrast between some terraces in the topographic image indicates that there are also steps half-unit cell high (an example is indicated by an arrow). The simplified drawing in Figure 3(c) pictures the YSZ film surface at the beginning of the deposition of a monolayer, half-unit cell high, covering terraces separated by steps mostly one or two unit cells high.

The epitaxial relationship between the YSZ(001) film and the STO(110) substrate was determined by XRD pole figure measurements done on the thickest film, 64 ML around asymmetrical STO(001) and YSZ(111) reflections using a two-dimensional detector. The pole figures (Figure 4(a)) indicate that the epitaxial relationship is [110]YSZ(001)//[001]STO(110), also supported by the observed RHEED patterns; thus, YSZ(001) grows epitaxially on the STO(110) substrate with the diagonals of the square YSZ(001) cell aligned with the [001] and [1–10] edges of the rectangular STO(110) cell and without in-plane crystal variants. The epitaxy is visualized in the schematic drawing presented in Figures 4(b)–4(d). The top view in Figure 4(b) shows the anisotropic matching between YSZ and STO. The YSZ:STO matching is 1:2 unit cells along STO[001] and 3:4 unit cells along STO[1–10]. The lateral views in Figures 4(c)

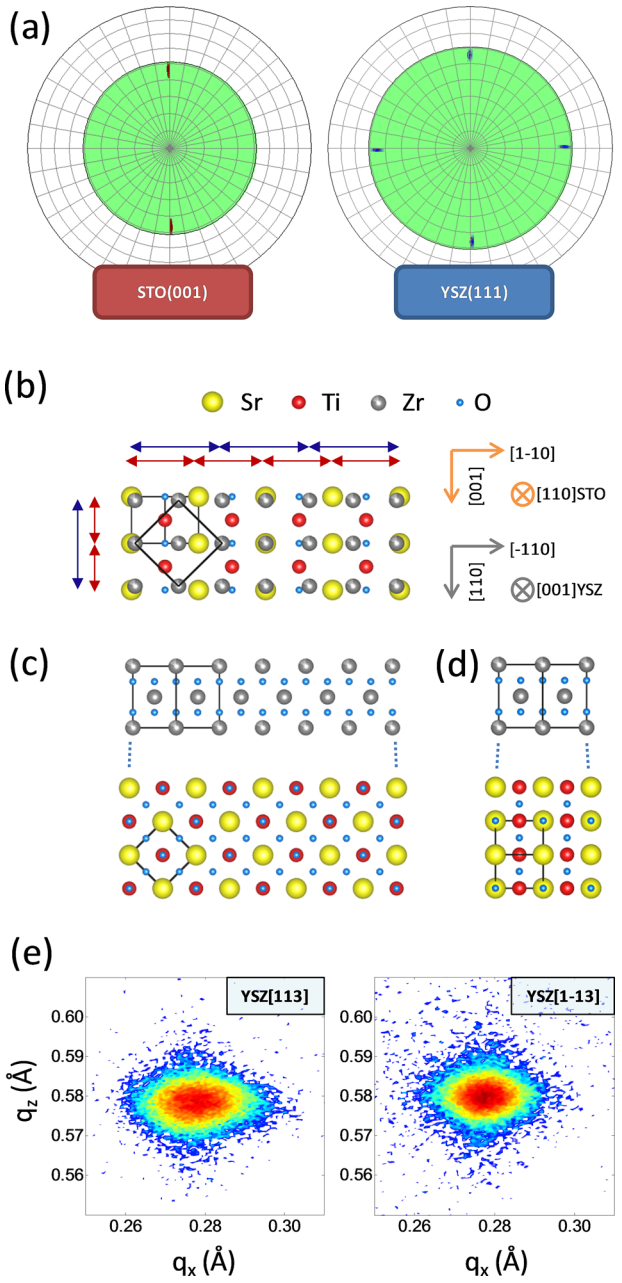

FIG. 4. (a) XRD pole figures around STO(001) and YSZ(111) asymmetric reflections of the 64 ML-thick YSZ film. (b)–(d) Schematic cartoons of the YSZ and STO crystal structures matching according to the [110]YSZ(001)// [001]STO(110) epitaxial relationship. (b) is a top view and (c) and (d) lateral views being the interface along STO[001] and STO[1–10], respectively. The arrows on the panel (c) indicate the unit cell size of YSZ (blue) and STO (red). (e) XRD reciprocal space maps around the (113) and (1–13) YSZ reflections of the 64 ML YSZ film.

and 4(d) illustrate the matching along STO[001] and STO[1–10], respectively. To obtain information on the strain state of the films, reciprocal space maps around YSZ(113) and (1–13) reflections were acquired (Figure 4(e)). Both reflections are found at the same absolute reciprocal space coordinates, with out-of-plane c = 5.17(1) Å and in-plane a = b = 5.09(1) Å cell parameters, indicating a tetragonal distortion.

The properties of the YSZ/STO interface are of the highest interest after the report of orders of magnitude enhancement of the ionic conductivity of ultrathin YSZ(001) films on STO(001) substrates.[17] It was proposed that the

heteroepitaxy of strained YSZ was possible in spite of the large lattice mismatch of 7% by disorder of the oxygen sublattice at the interface, with oxygen vacancies increasing the oxygen mobility.[17,18] In this context, beyond YSZ(001)/STO(001) interfaces, the growth of YSZ with dissimilar crystal orientation on top of STO may be instrumental to gain fundamental understanding on oxygen exchange across interfaces, and the role that structural symmetry can have on ionic diffusion. However, obtaining single domain YSZ films on STO substrates with orientation other than (001) has proved to be very challenging. For instance, Rivera-Calzada *et al.*[18] studied YSZ(110) films grown on STO(001) using low temperature and high rate deposition conditions, but the films presented structural domains and island growth. Conversely, it has been also reported that YSZ films on the STO(001) are either flat (001)-oriented or rough with tilted (111)-domains depending on the chemical termination, SrO or TiO_2, of the STO(001) substrates.[19] Then, the different approaches to obtain YSZ/STO(001) samples with symmetry discontinuity at the interface resulted in rough films with crystal variants. In contrast, here, we demonstrate a viable route towards two-dimensional growth of epitaxial single domain YSZ films, based on the reduction of the substrate symmetry. Dielectric spectroscopy measurements of the 32 ML thick sample (not shown) have evidenced large values of a frequency independent conductance along with a highly dispersive real part of the permittivity. This suggests an electronic contribution to the total conductivity which may be related to doping effects due to the incorporation of oxygen vacancies to the substrate. We cannot discard that the strong permittivity increase at low frequency might be related to an ionic contribution which would originate at the YSZ layers or their interfaces. Further, future work will be directed to conclude on the possible enhancement of ionic conduction at the YSZ/STO(110) interfaces.

In summary, single-domain F(h′k′l′)/S(hkl) oxide interfaces with symmetry discontinuity can be achieved, as it is confirmed with YSZ(001)/STO(110) interfaces. YSZ grows epitaxially by layer-by-layer mechanism with persistent RHEED oscillations up to a thickness above 15 nm. Although for the particular case of YSZ(001)/STO(110) the focus is on the possibility of ionic conductivity enhancement by oxygen vacancies, our results might allow exploring other interfaces. As an illustration, one could speculate whether strategies similar as those outline here could be instrumental to achieve F(h′k′l′)/S(hkl) for other interfaces. That would eventually allow analyzing the mismatch between electronic band structures for heterointerfaces with dissimilar symmetry, and explore their effects on physical properties.

Financial support by the Spanish Government [Project Nos. MAT2011-29269-CO3 and NANOSELECT CSD2007-00041] and Generalitat de Catalunya (No. 2009 SGR 00376) is acknowledged.

[1]D. G. Schlom, L. Q. Chen, C. B. Eom, K. M. Rabe, S. K. Streiffer, and J. M. Triscone, Annu. Rev. Mater. Res. **37**, 589 (2007).
[2]H. Y. Hwang, Y. Iwasa, M. Kawasaki, B. Keimer, N. Nagaosa, and Y. Tokura, Nature Mater. **11**, 103 (2012).
[3]A. Ohtomo and H. Y. Hwang, Nature **427**, 423 (2004).
[4]J. Chakhalian, A. J. Millis, and J. Rondinelli, Nature Mater. **11**, 92 (2012).
[5]G. Herranz, F. Sánchez, N. Dix, M. Scigaj, and J. Fontcuberta, Sci. Rep. **2**, 758 (2012).
[6]K. Ueda, H. Tabata, and T. Kawai, Science **280**, 1064 (1998).
[7]M. Grundmann, Phys. Status Solidi B **248**, 805 (2011).
[8]H. N. Lee, D. Hesse, N. Zakharov, and U. Gösele, Science **296**, 2006 (2002).
[9]F. Sánchez, R. Aguiar, V. Trítk, C. Guerrero, C. Ferrater, and M. Varela, J. Mater. Res. **13**, 1422 (1998).
[10]H. S. Kim, L. Bi, H. Paik, D. J. Yang, Y. C. Park, G. F. Dionne, and C. A. Ross, Nano Lett. **10**, 597 (2010).
[11]R. Bachelet, F. Valle, I. C. Infante, F. Sánchez, and J. Fontcuberta, Appl. Phys. Lett. **91**, 251904 (2007); F. Sánchez, C. Ocal, and J. Fontcuberta, Chem. Soc. Rev. **43**, 2272 (2014).
[12]D. Nečas and P. Klapetek, Cent. Eur. J. Phys. **10**, 181 (2012).
[13]K. Momma and F. Izumi, J. Appl. Crystallogr. **44**, 1272 (2011).
[14]C. Aruta, S. Amoruso, G. Ausanio, R. Bruzzese, E. Di Gennaro, M. Lanzano, F. Miletto Granozio, M. Riaz, A. Sambri, U. Scotti di Uccio, and X. Wang, Appl. Phys. Lett. **101**, 031602 (2012); C. Li, Q. Xu, Z. Weng, S. Zhang, A. Li, and D. Wu, *ibid.* **103**, 201602 (2013).
[15]J. A. Krogstad, M. Lepple, Y. Gao, D. M. Lipkin, and C. G. Levi, J. Am. Ceram. Soc. **94**, 4548 (2011).
[16]R. Bachelet, P. de Coux, B. Warot-Fonrose, V. Skumryev, J. Fontcuberta, and F. Sánchez, Thin Solid Films **519**, 5726 (2011).
[17]J. Garcia-Barriocanal, A. Rivera-Calzada, M. Varela, Z. Sefrioui, E. Iborra, C. Leon, S. J. Pennycook, and J. Santamaria, Science **321**, 676 (2008).
[18]A. Rivera-Calzada, M. R. Diaz-Guillen, O. J. Dura, G. Sanchez-Santolino, T. J. Pennycook, R. Schmidt, F. Y. Bruno, J. Garcia-Barriocanal, Z. Sefrioui, N. M. Nemes, M. Garcia-Hernandez, M. Varela, C. Leon, S. T. Pantelides, S. J. Pennycook, and J. Santamaria, Adv. Mater. **23**, 5268 (2011).
[19]A. Cavallaro, B. Ballesteros, R. Bachelet, and J. Santiso, CrystEngComm **13**, 1625 (2011).